Characterisation of Selective Laser Sintered Hydroxyapatite Based Biocomposite Structures for Bone Replacement

[1, 2]L. Hao, [1]M.M. Savalani, [3]Y. Zhang, [3]K.E. Tanner, [2]R.J. Heath, [2]R.A. Harris,

[1]School of Engineering, Computer Science and Mathematics, University of Exeter, EX4, 4QF, UK

[2]Loughborough University, Loughborough, Leicestershire, LE11 3TU, UK

[3]Department of Materials, Queen Mary University of London, London, E1 4NS, UK

Correspondence

Dr. Liang Hao
Lecturer,
School of Engineering, Computer Science and Mathematics,
University of Exeter,
Harrison Building,
Exeter EX4 4QF,
UK

Tel: + 44 (0) 1392 263665
Fax: + 44 (0) 1392 217965
Email: l.hao@exeter.ac.uk

Abstract

Integration of the bone into the implant is highly desirable for the long-term performance of the implant. The development of a bone-implant interface is influenced by the surface morphology and roughness, surface wettability and porosity of the implants. This study characterises such important properties of a hydroxyapatite based biocomposite structure fabricated by selective laser sintering with a comparison of a moulded specimen. The sintered specimens exhibited a rougher surface with open surface pores and a highly interconnected internal porous structure. It was shown that powder particles characteristics used in the selective laser sintering provided a more influential means to modify the surface morphology and the features of internal pores than laser parameter variation. The correlation of wettability and porous structure shows that although surface open pores could help cell ingrowth and bone regeneration, they resulted in a poorer wettability of the materials which may not encourage initial cell attachment and adhesion. The potential solution to improve the wettability and cell anchorage is discussed.

Keywords: *Selective laser sintering, hydroxyapatite, surface roughness, wettability, porosity, biocomposite structure*

1. Introduction

Customised implants provide the potential to improve bone defect repair methods and enhance the longevity of the implants by providing a more secure interlock due to exact geometry (Mercuri et al. 1995). Customized implants should be the first choice for the reconstruction of complex orbital fractures based on the good aesthetic and functional results, with significantly reduced operating times and morbidity in all cases (Hoffman et al. 1998) and more efficient surgery with a minimum adjustment (Ono et al. 1997) by utilizing a used pre-formed custom-made hydroxyapatite implants.

Integration of the bone into the implant is highly desirable characteristic for long-term performance and is influenced by the surface morphology and roughness, surface wettability and porosity of the implants. The alternations in surface morphology and roughness have been used to influence cell and tissue responses to implants (Puleo & Nanci 1999) and the rough surface provides mechanical interlocking (Fujimori 1995). The wettability generally presents the difference in surface chemistry and was shown to be one of the important factors for attachment differentiation of primary bovine osteoblasts (Meyer et al. 1993) and the protein adsorption and cell proliferation on the bio-inert ceramic (Hao & Lawrence 2004; Hao et al. 2004; Hao et al. 2005a; Hao et al. 2005d) and biocompatible metals (Hao et al. 2005b; Hao et al. 2005c). Recently, particular attention was paid to the synthesis of bioceramics with porous morphology to allow the ingrowth of bone tissue which further increases the mechanical fixation and integrity of the implant at the implantation site (Schnettler et al. 2003).

Medical applications and research in Rapid Manufacturing (RM), referring an additive layer-by-layer manufacturing process to produce an object, are driven by an individual's unique requirements of shape & functionality. Selective laser sintering (SLS) is an RM technique which operates by sequentially sintering a powdered material using heat supplied by selective exposure to a laser. Coole et al (Coole et al. 2005) showed that this process can be applied as an accurate method to directly make bone replacement materials using hydroxyapatite (HA) and poly-L-lactide (PLLA) polymer composite for the production of bespoke patient prosthesis. SLS was also investigated to produce bone scaffolds using polycaprolactone (PCL) (Williams et al. 2005), HA/polyetheretherketone (PEEK) (Tan et al. 2003) and HA/polyvinyl alcohol (PVA) (Chua et al. 2004).

Previous research has shown that SLS technique is capable of directly fabricating a clinical grade HA and high density polyethylene (HDPE) biocomposite (Hao et al. 2006b). Relatively high HA volume ratio (40 vol %) in HA-HDPE composites in the previous study resulted in insufficient mechanical properties to analyse the internal porous structure and pore interconnectivity. This study has used SLS to build HA-HDPE with 20 HA vol % content with acceptable mechanical properties and

characterised and analysed the internal pore structure, surface roughness and morphology and surface wettability of the products, all of which could effect the integration of implant with existing bone.

2. Methods

2.1 Material preparation and moulded specimen

The HDPE (Rigidex HD5226EA) was supplied in pellet form by BP Chemicals Ltd and synthetic HA particles (P218R, Plasma Biotal Ltd., UK) were used as the filler material for preparing 20 vol% HA-HDPE composites. The HA particles had a median size ($d_{0.5}$) of 3.80 μm. The mixture of HA and HDPE, at 20 vol% HA, was compounded in a twin screw extruder (Betol BTS40L, Betol, Luton, UK) to produce composites. The extruded composite was subsequently pelletized in a Betol pelletizer and then powderized in an ultra centrifuge mill (Retsch powderizer, Germany) using a sieve of 0.120 mm aperture size. The resultant particles were then sieved using sieves with aperture size of 105 μm and powders with particle size (PS) of $0 < PS < 105$ μm and 105 μm $< PS$ were obtained. For comparison, full dense materials were compression moulded by hot press machine at 215 ^{o}C (Bradley & Turton Ltd, England) and moulded plates were then cut into required dimensions.

2.2 SLS experimental systems and processing

A bespoke experimental system for the sintering of polymer / ceramic biomaterials incorporates an experimental powder bed chamber and a CO_2 laser system (Synrad, Ltd, USA) described in previous work (Hao et al.). The rectangular specimens with 3 × 21 mm dimension were built up with six SLS sintered layers with 0.15 mm layer thickness. Three different laser powers at fixed laser scanning speed of 3.6 m s^{-1} is used, while other processing conditions were kept constant with 128 °C powder bed temperature and 63 μm laser scanning spacing.

2.3 Characterisation

The surface roughness (R_a) of the HA-HDPE was measured by a Talysurf 4 (Taylor Hobson, England). The surface morphologies of specimens were examined using a scanning electron microscope (SEM) (LEO 440, UK). Advancing contact angle measurements were measured by the sessile drop method using contact angle instrument (OCA20, Dataphysics Instruments GmbH) for the moulded specimen and laser sintered specimens. The tested liquids used were water, diiodomethane and simulated body fluid (SBF) (Kokubo et al. 1990). The cross-sections of the specimens were prepared by penetrating and mounting the cross-sectioned specimens using red resin (Epocolour, Buehler UK). The specimens were clipped and submerged and infiltrated in a vacuum condition. The

mounted specimens were set overnight and then polished to obtain the required cross sections for optical microscopy analysis. The images of the cross-section specimen were processed to contrast the sintered composite and the filled resin under ImageJ software (ImageJ 1.34S, USA) and the percentage of pores in the cross-section were calculated. Mean values were derived from eight measurements from the cross-sectional images for the specimens sintered at each parameter. The porosity of the specimens is also obtained by weight and volume measurement.

3. Results

The primary difference among two kinds of HA-HDPE composite powders is their particle size and shape (See Figure 1). The large particle powderS exhibit very irregular morphology, while, the small particle powders are less irregular and certain portion of them look relatively spherical.

As shown in

Table 1, the R_a of laser sintered specimens is greater than the moulded specimen. The laser power variation generated minor differences in R_a. A lower R_a value appears on the specimens sintered with small particles compared with those with large particles for the same laser power is used.

The moulded specimen exhibits a flat and smooth surface without any void or pores and the typical surface morphologies of the laser sintered specimens are rough and have a lot of pores (see Figure 2). When the small particles were used (Figure 2 (b), (d), (f)), the particles present on the surface fused significantly and boundaries between particles became largely indistinguishable. Some pores with typical size less than 100 μm were distributed among the fused particles on these specimens' surface. The change of laser power did not result in considerable difference in the degree of particles' fusion and the size and morphology of the surface pores. When the larger particles were used Figure 2(c), (e), (g), the particles exhibited contact networking and fused partially together. A few incidences of contact networking were observed between the particles and some individual particles could still be identified on the surface of the specimens sintered at the laser power of 3.6 W. The degree of contact networking and fusion increased with the laser power. A number of pores among the contacted particles were observed and some pores were larger than 100 μm.

The cross-sectional images exhibit the internal structure of the laser sintered HA-HDPE specimens using different laser powers and particles (see Figure 2.). The lighter colour area is the pores which were penetrated by the resin. The fact that the resin filled in all the pores implies that the pores inside

the specimens are interconnected as any closed pores would not be infiltrated by resin. Some pore areas are connected with others and these porous structures are generally irregular in shape and vary in size. The area of the occupied by the pores ranges from 23.2 to 39.3 % as calculated using image J software and the porosity determined by the fraction of weight by volume ranges form 45.4 to 54.3 % (see Figure 3.). Comparing the specimens sintered at the same laser settings at 3.6, 4.8 and 6.0 W, the size of the pores and the area they occupy in the specimens sintered with large particles are generally larger than those with small particles. At 3.6 W power, the maximum value of the connected pore channel width estimated by intercept method is approximately 70 μm for the specimen sintered with small particles and 150 μm for the specimen sintered with large particles (Figure 2. (a)(b)). When the same particles were used, the size of the pores and the area they occupied in the specimens decreased with increased laser power.

An optical micrograph of an advanced sessile drop of water (see Figure 5) reveals that there is obvious difference in the value of θ using water between the moulded and sintered specimen. The water θ is 85.2 °C for the moulded specimen, indicating that it is wettable by water. Water did not wet the sintered specimen with θ of 122.3 °C. With all the test liquids used the sintered specimens experienced a signification increase in θ compared with the moulded specimens (see Table 2). For the sintered specimens fabricated at same laser power, θ is greater on the specimens sintered with large particles than those with small particles. For the specimens sintered with the same particles, the increase in laser power did not include a constant change in θ for all the test liquids.

4. Discussion

4.1. The effect of the laser power and particle sizes

Laser sintered specimens had rougher surfaces than the moulded specimens. This difference is likely to be due to the interaction time between the laser beam and powder particles being too short and the melted or partially melted powder particles were not able to flow and flatten the surface. Due to the very irregular morphology exhibited by the large particles, the use of these particles resulted in the rougher surface compared those with small particles. The laser power did not present a constant relationship with surface roughness on account of the large irregularity of the particles used. This indicates that the particles' size play a more important role in surface roughness than the laser parameters. The rougher surface of the laser sintered specimens should better provide mechanical interlocking in implant applications. Surface roughness could mediate the cell adhesion. Dalby et al (Dalby et al. 2000) have found that the surface topographies of HA-HDPE effects significantly on cell

attachment and subsequent cellular behaviour in relation to proliferation and faster and greater cell attachment was shown on the optimized topography following polishing and roughening.

The degree of the particles' fusion could be influenced by the laser parameter and different particles. The specimens sintered with small particles exhibited more particle fusion compared with those sintered with large particles. This is likely to be due to finer powder particles resulting in the higher sintering activity and greater densification and agree with previous study that the smaller iron powder particles experience greater densification due to the increased sintering activity (Simchi 2004). The number of pores and size of pores on the specimens sintered with large particles are larger than those on the specimens sintered with small particles. This may be because the interfacial space among the small particles was much smaller and the degree of the fusion and densification of these particles were larger compared large particles. The increased heat energy induced by increasing laser power resulted in the enhancement of the particle contact network and greater fusion with larger particles (see Figure 3). But, the change in laser power did not bring about a marked difference in the surface porosity and morphology of specimens sintered with small particles. These results show that the effect of the particle size on the pore size and morphology is greater than the laser power. Hence, the surface morphology and pore size can be modified by using different particles, and a subsequent biological response may be mediated by these controlled porous structures. The surface porosity may provide the necessary topology for cell ingrowth into implant and may also facilitate an initial anchoring of the implant within the newly formed bone. This was demonstrated on the laser-textured and surface blasted Ti6Al4V alloy implants preferentially used the pores to anchor the implant (Gotz et al. 2004).

Implants need to possess an open-pore geometry with a highly porous surface and interconnected internal porous microstructure that allows cell in-growth and reorganization and provides the necessary space for neovascularization from the surrounding tissues *in vivo*. The porosity and degree of pore interconnectivity directly affect the diffusion of physiological nutrients and gases and the removal of metabolic waste and by-products from cells that have grown in the implant (Leong et al. 2003). The deliberate and controlled porosity would further mean that even if the initial implant strength and toughness were below that required for long-term use, the ingrown bone would increase the strength of the bone-implant composite by a factor of 3 or 4 (Hing et al. 2004). The internal pores are highly connected in the laser sintered specimens. This may be partly due to the fact that the powders are subjected to low compaction forces during their deposition to produce the new layers. With increased laser power and the amount of energy, the pore size and porous area decreased in the specimens when the same particles were used due to the higher degree of particle fusion. Previous studies also revealed that the porosity of polymeric matrix drug delivery decreased as laser power increased (Leong et al. 2001). The pore size and porous area also depend on the particles'

morphology. The specimens sintered with large particles present less compaction and thus higher porosity compared with those with small particles when the same laser power was used. The formation of internal pores is influenced by the compact density and space among the particles which are determined by the characteristics of the powder particles and powder lay down process. The internal pores fabricated in this study are irregular and homogeneous because the particles used are largely irregular. The size of pores in the specimens fabricated in this study was generally in a range from 10 to 200 μm. Such pores present a micro-environment which effect individual cells (10 μm), functional subunits (100 μm) (Liu Tsang & Bhatia 2004), nutrient provision and vascularisation (200 – 500 μm) (Xiong et al. 2001). The fact that the connected pore channel width in the sintered with large particles was much larger than those with small particles at 3.6 W power indicates that the size of powder particles play an important role in determining the feature of internal pores. This is likely to be because particles' size effects the packing density of the layered powders and predominantly determines the internal space existing among the particles. These results indicate that the size and channel width of pores can be controlled by varying the size and characteristics of powder particles. Some studies recommend the minimum pore size for a tissue scaffold is 100 μm for bone tissue regeneration (Karageorgiou & Kaplan 2005) and high porosity and interconnectivity is needed for tissue scaffold (Leong et al. 2003). The result suggests that the use of large particles in SLS enable the production of specimens which could have large proportion of optimum sized pores to encourage bone tissue ingrowth. However, it is necessary to be aware that the degree of inter-particulate sintering and mechanical strength can be deteriorated with increased powder particle size. The balance between the porosity and mechanical properties of specimens needs to be considered to choose the proper powder particle topology. The results reveal that the SLS process may provide multiple means to control the internal structure of HA-HDPE composite material by varying the process parameters and the powder particle topology.

4.2. Wettability and correlation with porous structure

The apparent contact angles for all the test liquids on the laser sintered specimens are higher than the moulded specimen, indicating a poorer wettability of sintered specimens compared with the moulded specimen. The surface roughness and open pore surface of the sintered specimen may be the factors governing the modification of wettability of the sintered specimens. Generally, the wettability of a surface is associated with its roughness for a certain material. Wenzel's equation (Wenzel 1936) shows that high roughness will enhance both hydrophobicity of hydrophobic surface and hydrophilicity of hydrophilic surfaces. The sintered specimens exhibited higher surface roughness than the moulded specimen. This can contribute to the

enhanced SBF θ on the sintered specimens compared with moulded specimens. However, other two test liquids of water and diiodomethane did not present this agreement. The θ of these liquids were lower than 90° for the moulded specimen, indicating the material was wettable by these liquids. However, θ still increased for the sintered rougher specimens, implying the wettability decreased. Hence, surface roughness could not be the predominant factor governing the change in wettability.

The presence of the pores in the sintered specimens could be the primary reason for the difference between the θ on sintered specimens and moulded specimen. This can be proved by using Cassie and Baxter equation (Cassie & Baxter 1944), which for a solid having two different types of areas takes the form

$$\cos\theta = f_1 \cos\theta_1 + f_2 \cos\theta_2 \qquad (1)$$

where θ is the apparent contact angle observed on the porous solid surface, θ_1 and θ_2 are the contact angles corresponding to the type 1 and 2 areas, respectively, and f_1 and f_2 are the fractional areas of type 1 and 2 areas, respectively. For the porous solid with f_1 being the fractional area of a flat surface of a given contact angle θ_1 and f_2 the fractional area of void, θ_2 would be 180°. Taking into account that $f_1 = 1\text{-}f_2$, Equation (1) can be rewritten as follows

$$\cos\theta = (1 - f_2)\cos\theta_1 - f_2 \qquad (2)$$

Equation (2) predicts the poorer wettability, i.e. $\theta > \theta_1$, for a non-wetted porous surface, for which the liquid does not penetrate the pores. In this case, θ_1 is for the moulded specimen and θ is for the porous laser sintered specimens. The fractional area of void (pore) plays a significant and predominant role in reducing the apparent wettability of the sintered specimens. The higher the surface porosity, the lower the wettability is. A linear relationship was found for the θ and the pore volume fraction for the water, diiodomethane and SBF test liquids (see Figure 5.). This may explain the finding that the specimens sintered with large particles, which exhibited higher surface porosity, have a lower wettability than the specimens with small particles. The larger the θ_1 is, the larger difference between θ and θ_1. This explains that there are considerable differences in the θ for the water and SBF liquids between the sintered and moulded specimen, whereas, only a slight difference for diiodomethane.

It has been mentioned that optimum bone implants need to possess an open-pore geometry with a highly porous surface and internal porous microstructure. However, the highly porous surface introduces in the poorer wettability to this material. Generally, the hydrophobic surface lack cell recognition signals and do not encourage cell attachment. Hence, the sintered specimens with highly porous surface might not stimulate the initial cell adhesion. But open surface pores allow the

infiltration of protein such as collagen. It showed that collagen adsorption not only enhances the hydrophilicity of the porous scaffold structure, but also enables the polar groups introduced into the surfaces which encourage the anchorage of cells (Yang et al. 2002.). Thus, infiltration of collagen and other bio-growth factors into surface and internal pores are recommended for the laser sintered structures.

5. Conclusions

Compared with a mould specimen, laser sintered specimens exhibited a rougher and more open pored surface, a highly interconnected internal porous structure and a lower apparent wettability. Both laser power and particle size influence the properties of the laser sintered specimen. The specimen sintered with large particles showed higher surface roughness and larger and more surface pores than that sintered with small particles, whereas the laser power does not present a constant effect on the surface morphology. This indicates that the powder particle topology plays a predominant role in surface morphology. The laser sintered specimens presented highly interconnected porous structures revealed by the cross-sectional analysis. The percentage of the internal porous area increases with the increased particle size and the decreases with the increased laser power. The poorer wettability of the sintered specimens resulted from the open pore surface as explained by the Cassie and Baxter equation.

Acknowledgements

The authors would like to express their gratitude for financial support from the UK Department of Health's New & Emerging Applications of Technology (NEAT E059) programme.

References

Cassie, A. B. D. & Baxter, S. 1944 Wettability of porous surfaces. *Transactions of the Faraday Society* **40,** 546 - 551.

Chua, C. K., Leong, K. F., Tan, K. H., Wiria, F. E. & Cheah, C. M. 2004 Development of tissue scaffolds using selective laser sintering of polyvinyl alcohol/hydroxyapatite biocomposite for craniofacial and joint defects. *Journal of Materials Science: Materials in Medicine* **15,** 1113-1121.

Coole, T., Cruz, F., Simoes, J. & Bocking, C. 2005 Customistaion of bio-cermic implants using SLS. In *The 2th International Conference of Virtual Modelling and Rapid Manufacturring* (ed. J. B. Paulo), pp. 147 - 151. Leiria, Portugal: Taylor & Francis Group.

Dalby, M. J., Kayser, M. V., Bonfield, W. & Di Silvio, L. 2002 Initial attachment of osteoblasts to an optimised HAPEXT^{M} topography. *Biomaterials* **23,** 681-690.

Fujimori, S. 1995 Surface characterization of titanium plates with different surface treatments and cellular proliferation and expression of osteoblast-like cells in vitro on their surface. *Journal of Dental Materials* **14,** 155-168.

Gotz, H. E., Muller, M., Emmel, A., Holzwarth, U., Erben, R. G. & Stangl, R. 2004 Effect of surface finish on the osseointegration of laser-treated titanium alloy implants. *Biomaterials* **25,** 4057-4064.

Hao, L. & Lawrence, J. 2004 On the role of CO_2 laser treatment in the human serum albumin and human plasma fibronectin adsorption on zirconia (MgO-PSZ) bioceramic surface. *Journal of Biomedical Materials Research* **69A,** 748-756.

Hao, L., Lawrence, J. & Chian, K. S. 2004 On the effects of CO_2 laser irradiation on the surface properties of a magnesia partially stabilised zirconia (MgO-PSZ) bioceramic and the subsequent improvements in human osteoblast cell adhesion. *Journal of Biomaterials Application* **19,** 81-105.

Hao, L., Lawrence, J. & Chian, K. S. 2005a Osteoblast cell adhesion on laser modified zirconia based bioceramic. *Journal of Materials Science: Materials in Medicine* **16,** 719-726.

Hao, L., Lawrence, J. & Li, L. 2005b The manipulation of the osteoblast cell response to the Ti-6Al-4V titanium alloy using high power diode laser (HPDL). *Applied Surface Science* **247,** 602-606.

Hao, L., Lawrence, J., Phua, Y. F., Chian, K. S., Lim, G. C. & Zheng, H. Y. 2005c Enhanced human Osteoblast cell adhesion and proliferation on 316 LS stainless steel by means of CO2 laser surface treatment. *Journal of Biomedical Materials Research B, Applied Biomaterials* **73B,** 148-156.

Hao, L., Ma, D. R., Lawrence, J. & X., Z. 2005d Enhancing osteoblast functions on a magnesia partially stabilised zirconia bioceramic by means of laser irradiation. M*aterials Science & Engineering C: Biomimetic and Supramolecular Systems* **25,** 496 - 502.

Hao, L., Savalani, M. M., Zhang, Y., Tanner, K. E. & Harris, R. A. 2006a The effect of material and processing conditions on characteristics of hydroxyapatite and high density polyethylene bio-composite by selective laser sintering. *Proceedings of the IMechE Part L, Journal of Materials: Design & Application,* **220**, 125-137**.**

Hao, L., Savalani, M. M., Zhang, Y., Tanner, K. E. & Harris, R. A. 2006b Selective laser sintering of hydroxyapatite reinforced polyethylene composites for bioactive implants and tissue scaffold development. *Proceedings of the IMechE Part H, Journal of Engineering in Medicine* **220,** 521 - 531.

Hing, K. A., Best, S. M., Tanner, K. E., Bonfield, W. & Revell, P. A. 2004 Mediation of bone ingrowth in porous hydroxyapatite bone graft substitutes. *Journal of Biomedical Materials Research Part A* **68A,** 187-200.

Hoffman, J., Cornelius, C. P., Groten, M., Probster, L., Pfannenberg, C. & Schwenzer, N. 1998 Orbital reconstruction with individually copy - milled ceramic implants. *Plastic Reconstruction Surgery* **101,** 604-612.

Karageorgiou, V. & Kaplan, D. 2005 Porosity of 3D biomaterial scaffolds and osteogenesis. B*iomaterials* **26,** 5474-5491.

Kokubo, T., Kushitani, H., Sakka, S., Kitsugi, T. & Yamamuro, T. 1990 Solutions able to reproduce in vivo surface-structure changes in bioactive glass-ceramic A-W$^{3.}$ *Journal of Biomedical Materials Research* 2**4,** 721-734.

Leong, K. F., Cheah, C. M. & Chua, C. K. 2003 Solid freeform fabrication of three-dimensional scaffolds for engineering replacement tissues and organs. *Biomaterials* 2**4,** 2363-2378.

Leong, K. F., Phua, K. K. S., Chua, C. K., Du, Z. H. & Teo, K. O. M. 2001 Fabrication of porous polymeric matrix drug delivery devices using the selective laser sintering technique. *Proceedings of the Institution of Mechanical Engineers, Part H: Journal of Engineering in Medicine* **215,** 191-201.

Liu Tsang, V. & Bhatia, S. N. 2004 Three-dimensional tissue fabrication. *Advanced Drug Delivery ReviewsIntelligent Therapeutics: Biomimetic Systems and Nanotechnology in Drug Delivery* **56,** 1635-1647.

Mercuri, L. G., Wolford, L. M., Sanders, B., White, D., Hurder, A. & Herderson, W. 1995 Custom CAD/CAM total temporomandibular joint reconstruction system: preliminary multicenter report. *Journal of Oral Maxillofacial Surgery* **53,** 106-115.

Meyer, U., Szulczewski, D. H., Moeller, K., Heide, H. & Jones, D. B. 1993 Attachment kinetics and differentiation of osteoblasts on different biomaterials. *Cells and Materials* **3,** 129-140.

Ono, I., Tabteshita, T., Satou, M., Sasaki, T., Matsumoto, M. & Kodama, N. 1997 Treatment of large complex cranial bone defects by using hydroxyapatite ceramic implants. *Plastic Reconstruction Surgery* **104,** 339 - 349.

Puleo, D. A. & Nanci, A. 1999 Understanding and controlling the bone-implant interface. *Biomaterials* **20,** 2311-2321.

Schnettler, R., Alt, V., Dingeldein, E., Pfefferle, H.-J., Kilian, O., Meyer, C., Heiss, C. & Wenisch, S. 2003 Bone ingrowth in bFGF-coated hydroxyapatite ceramic implants. *Biomaterials* **24,** 4603-4608.

Simchi, A. 2004 The role of particle size on the laser sintering of iron powder. *Metallurgical and Materials Transactions B: Process Metallurgy and Materials Processing Science* **35,** 937-948.

Tan, K. H., Chua, C. K., Leong, K. F., Cheah, C. M., Cheang, P., Abu Bakar, M. S. & Cha, S. W. 2003 Scaffold development using selective laser sintering of polyetheretherketone-hydroxyapatite biocomposite blends. *Biomaterials* **24,** 3115-3123.

Wenzel, R. N. 1936 Resistance of solid surfaces to wetting by water. *Industrial Engineering Chemistry* **28,** 988-994.

Williams, J. M., Adewunmi, A., Schek, R. M., Flanagan, C. L., Krebsbach, P. H., Feinberg, S. E., Hollister, S. J. & Das, S. 2005 Bone tissue engineering using polycaprolactone scaffolds fabricated via selective laser sintering. *Biomaterials* **26,** 4817-4827.

Xiong, Z., Yan, Y., Zhang, R. & Sun, L. 2001 Fabrication of porous poly(-lactic acid) scaffolds for bone tissue engineering via precise extrusion. *Scripta Materialia* **45,** 773-779.

Yang, J., Bei, J. & Wang, S. 2002 Enhanced cell affinity of poly (,-lactide) by combining plasma treatment with collagen anchorage. *Biomaterials* **23,** 2607-2614.

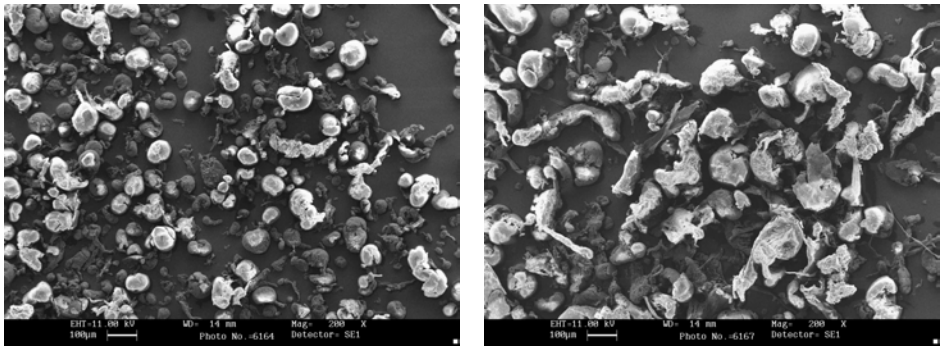

(a) (b)

Figure 1. SEM images of HA/HDPE powders with different sizes (a) 0 < PS < 105 μm, (b) 105 μm < PS (marker bars = 100 μm).

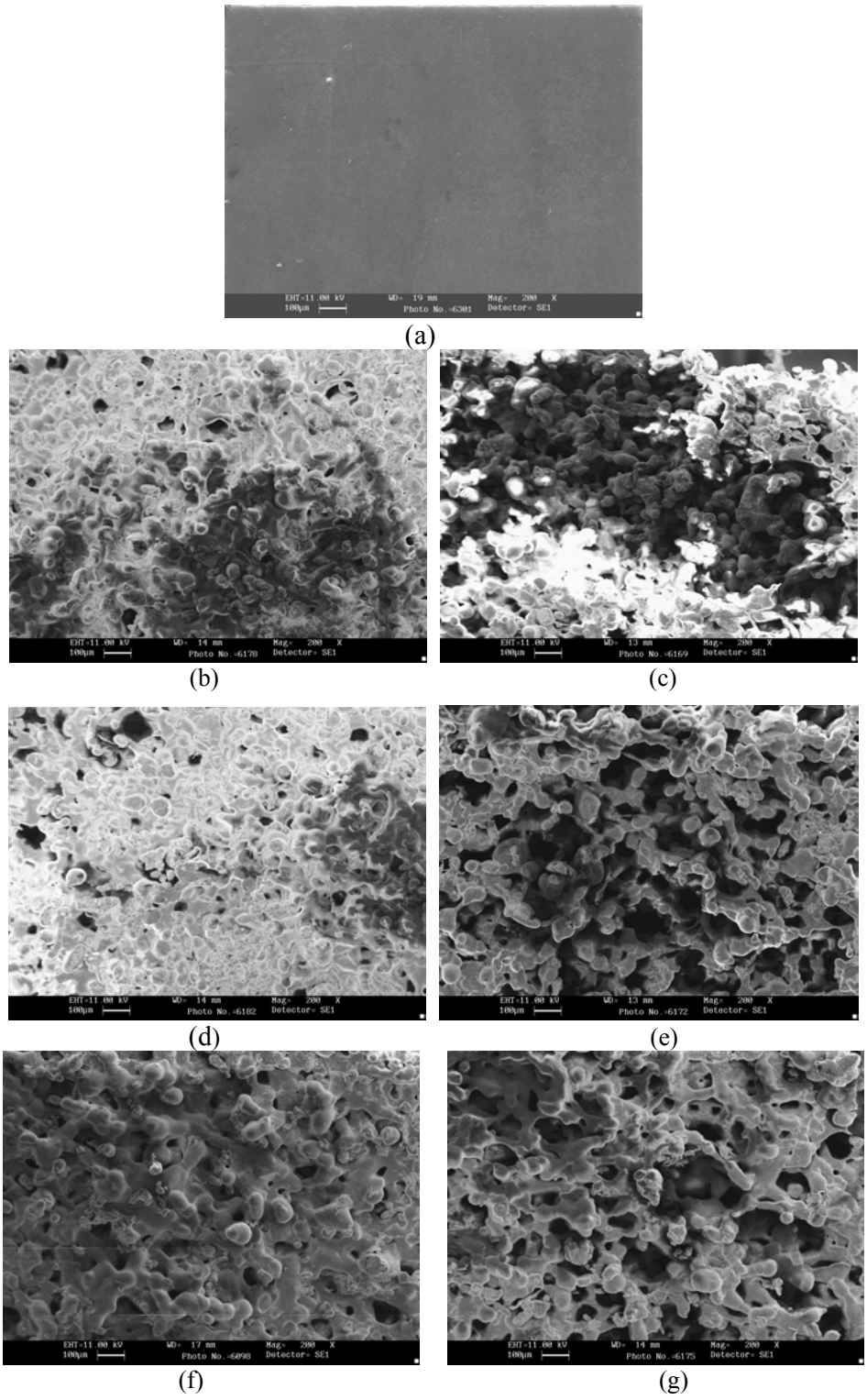

Figure 2. SEM surface images of (a) moulded HA-HDPE specimen and laser sintered specimens at scanning speed of 3600 mm s^{-1} at different laser power and particle size *(b) 3.6 W, 0 < PS < 105 μm, (c) 3.6 W, 105 μm < PS, (d) 4.8 W, 0 < PS < 105 μm, (e) 4.8 W, 105 μm < PS (f) 6.0 W, 0 < PS < 105 μm; (g) 6.0 W, 105 μm < PS (marker bars = 100 μm).*

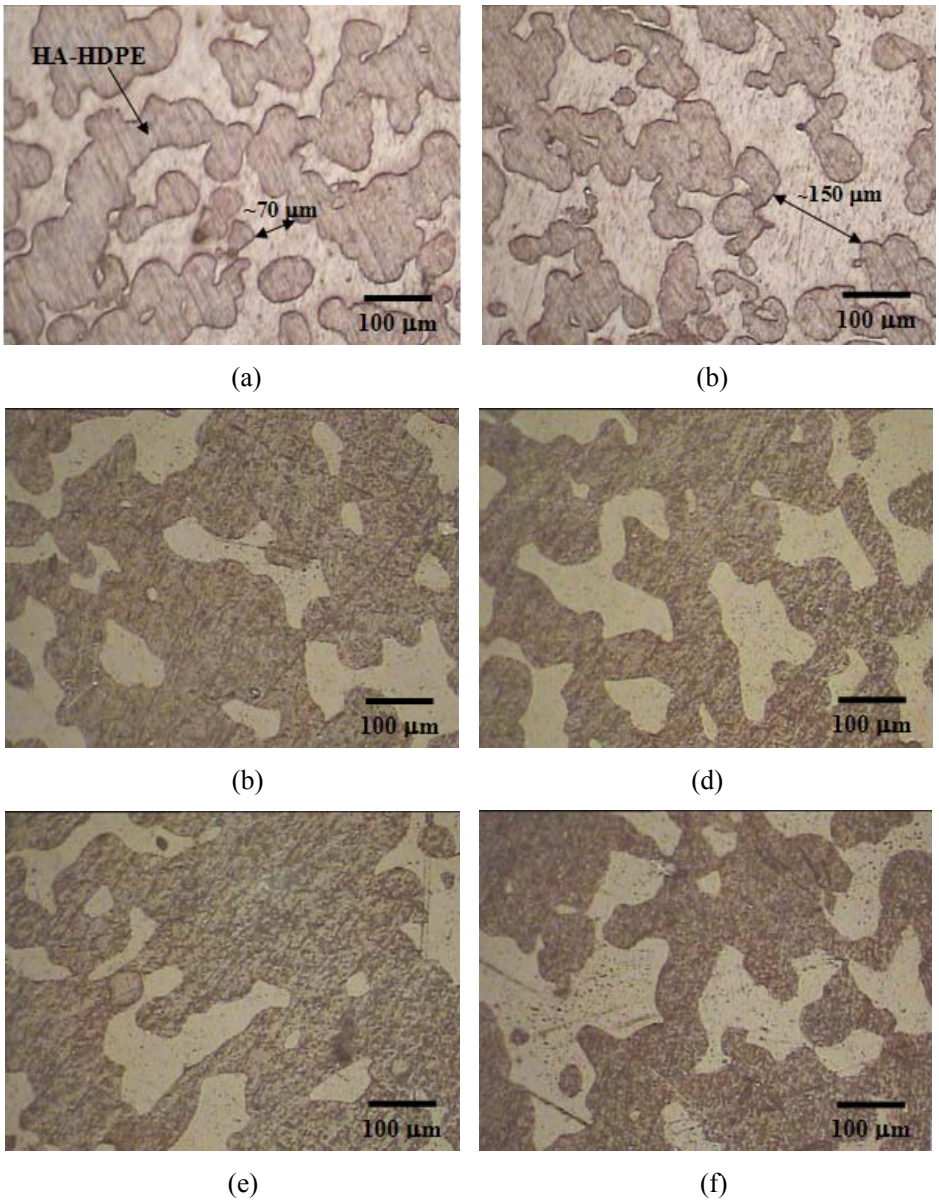

Figure 3. Typical optical images of the cross-section of the HA-HDPE specimens at scanning speed of 3600 mm s^{-1} at different laser power and particle size (a) 3.6 W, 0 < PS < 105 µm, (b) 3.6 W, 105 µm < PS, (c) 4.8 W, 0 < PS < 105 µm, (d) 4.8 W, 105 µm < PS (e) 6.0 W, 0 < PS < 105 µm; (f) 6.0 W, 105 µm < PS.

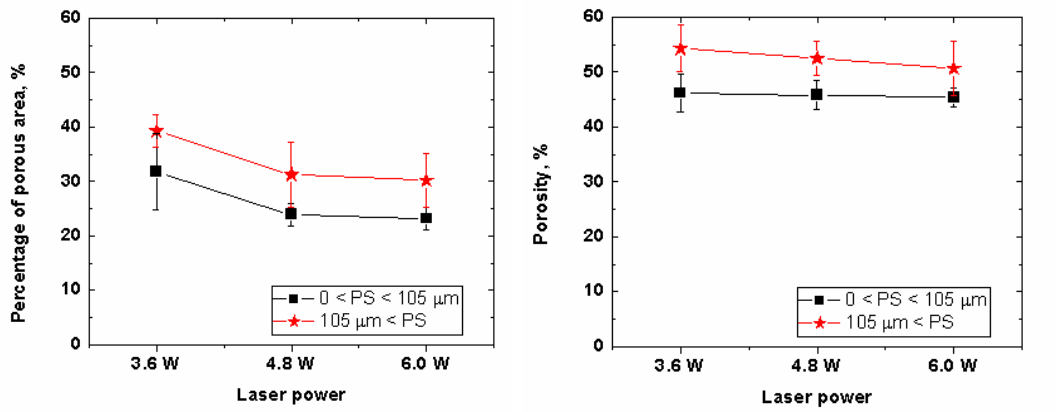

(a) (b)

Figure 4. The percentage of internal porous area (a) and porosity determined by the fraction of weight by volumne of the specimens sintered at different laser power and with different particles

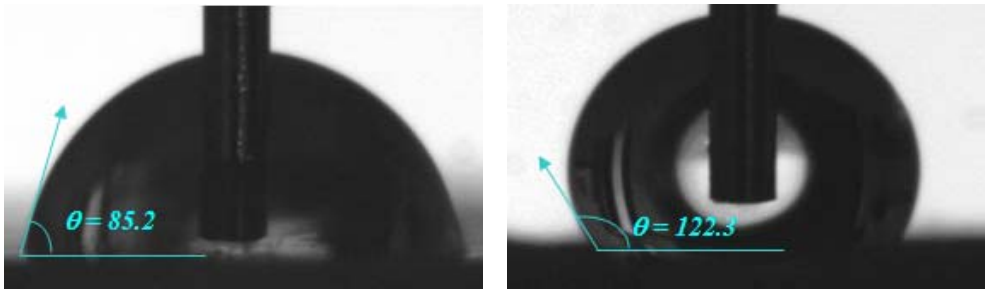

(a) (b)

Figure 5. Contact angle, θ, of water on the moulded HA-HDPE specimen (a) and laser sintered specimen (b) at laser power of 6.0 W and particle size of 0 < PS < 105µm.

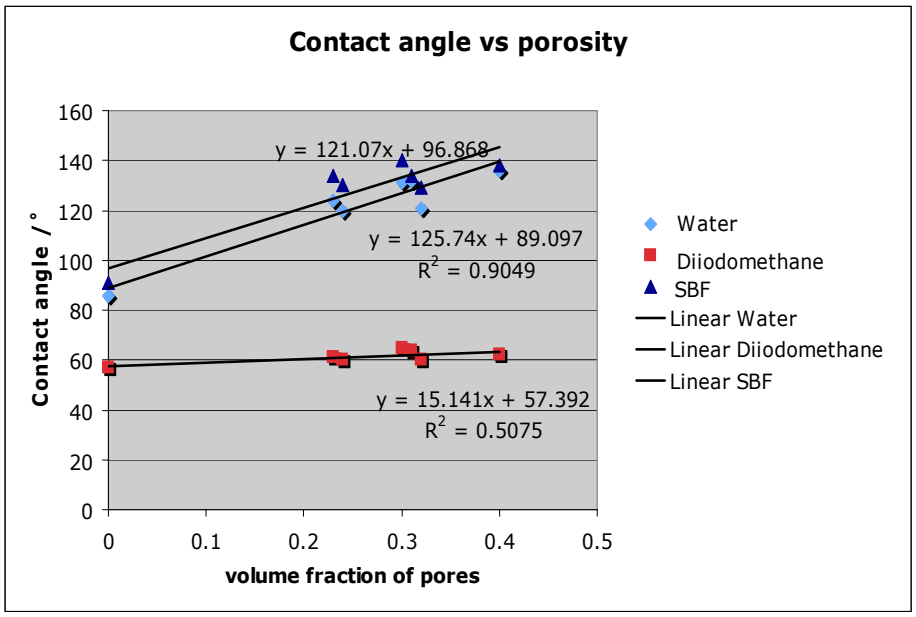

Figure 6. The relationship between the contact angle and volume fraction of pores in SLS fabricated component.

Table 1. The surface roughness of the specimens sintered at different laser power and using difference particles

Specimens	**Surface roughness, R_a (μm)**	
Laser power	**Particle Size PS**	
	0< PS <105 μm	**105 μm < PS**
3.6 W	12.83 ± 1.82	14.32 ± 1.64
4.8 W	13.74 ± 1.91	14.56 ± 1.69
6.0 W	13.61 ± 2.01	14.76 ± 1.09
Moulded specimen	1.61 ± 1.11	

Table 2. Contact angle of water, diiodomethane, SBF test liquids on the specimens (*P1= 0 < PS < 105μm, P2 = 105 μm < PS).*

Specimens	***Contact angle (deg)***					
Laser power	**Water**		**Diiodomethane**		**SBF**	
	P1	**P2**	**P1**	**P2**	**P1**	**P2**
3.6 W	121 ± 2	136 ± 5	60 ± 3	62 ± 3	129 ± 2	138 ± 2
4.8 W	120 ± 2	132 ± 3	60 ± 4	64 ± 3	130 ± 1	134 ± 1
6.0 W	124 ± 3	131 ± 4	61 ± 2	65 ± 3	134 ± 1	140 ± 3
Moulded specimen	86 ± 2		57 ± 1		91 ± 1	

.